Check for updates

Received: 14 May 2022 | Revised: 18 August 2022 | Accepted: 16 September 2022

DOI: 10.1002/pip.3627

RESEARCH ARTICLE

PROGRESS IN PHOTOVOLTAICS WILEY

Atomic scale controlled tunnel oxide enabled by a novel industrial tube-based PEALD technology with demonstrated commercial TOPCon cell efficiencies > 24%

Baochen Liao[1,2] | Weiliang Wu[3] | Reuben J. Yeo[4] | Xinyuan Wu[5] | Sheng Ma[6] | Qiang Wang[1] | Yimao Wan[7] | Xiaodong Su[8] | Wenzhong Shen[6] | Xiang Li[2] | Weimin Li[2] | Guoqiang Xing[3] | Bram Hoex[5]

[1]School of Information Science and Technology, Nantong University, Nantong, Jiangsu, China

[2]Jiangsu Leadmicro Nano Technology Co., Ltd., Wuxi, Jiangsu, China

[3]Tongwei Solar Co., Ltd., Meishan, Sichuan, China

[4]Institute of Materials Research and Engineering (IMRE), Singapore

[5]School of Photovoltaic and Renewable Energy Engineering, University of New South Wales, Sydney, New South Wales, Australia

[6]Institute of Solar Energy, Shanghai Jiao Tong University, Shanghai, China

[7]Risen Energy Co., Ltd., Ningbo, Zhejiang, China

[8]School of Physical Science and Technology, and Jiangsu Key Laboratory of Thin Films, Soochow University, Soochow, Jiangsu, China

Correspondence
Baochen Liao, School of Information Science and Technology, Nantong University, Jiangsu 226019, China.
Email: liaobaochen@ntu.edu.cn

Weiliang Wu, Tongwei Solar Co., Ltd., Meishan, Sichuan, 620010, China.
Email: wuwl02@tongwei.com

Reuben J. Yeo, Institute of Materials Research and Engineering (IMRE), 138635, Singapore.
Email: reuben_yeo@imre.a-star.edu.sg

Weimin Li, Jiangsu Leadmicro Nano Technology Co., Ltd., Wuxi, Jiangsu 214028, China.
Email: weiming.li@leadmicro.com

Funding information
the Research Funding for High-level Talents of Nantong University, Grant/Award Number: 03083035; the Major Program for the Natural Science Research of the Higher Education Institutions of Jiangsu Province, China, Grant/Award Number: 19KJ320004; the Construction Fund for School of Tongke Microelectronics, Nantong University, Grant/Award Number: 0702610104; the Research Funding for Jiangsu Specially-Appointed Professor, Grant/Award Number: 06210061007

Abstract

In this work, we report on a significant breakthrough in fabricating the critical tunnel oxide layer of tunnel oxide passivated contacts (TOPCon) high-efficiency solar cells compatible with high-volume manufacturing. We show that the tunnel oxide can be controlled at the atomic scale, enabled by an innovative tube-type industrial plasma-assisted atomic layer deposition (PEALD) method. In combination with an in situ doped poly-Si (n^+) layer grown by plasma-enhanced chemical vapor deposition, a uniform, ultrathin ~1.3 nm SiO_x layer is obtained at the c-Si/SiO_x/poly-Si (n^+) interface. Extremely low recombination current densities down to 2.8 fA/cm^2 and an implied open-circuit voltage (iV_{oc}) as high as 759 mV are achieved, comparable to state-of-the-art laboratory results. The developed tube-type PEALD SiO_x is applied to industrial TOPCon solar cells resulting in a solar cell efficiency and open-circuit voltage of up to 24.2% and 710 mV, respectively. The tunnel oxide process window is about 2.4 Å, highlighting the importance of precisely controlling the tunnel oxide thickness at the atomic scale for TOPCon solar cells. The newly developed tube-type industrial PEALD SiO_x method opens up a promising new route toward mass production of high-efficiency industrial TOPCon solar cells. Furthermore, the developed tube-type PEALD method can easily be integrated with the industrial tube-type plasma-enhanced chemical vapor deposition (PECVD) method, thus enabling the deposition of all thin film layers in TOPCon solar cells in one integrated PEALD/PECVD system. This significantly simplifies manufacturing complexity and fosters the commercialization of next-generation high-efficiency industrial TOPCon solar cells.

 © 2022 John Wiley & Sons Ltd.

KEYWORDS
ASC-TOPCon, PECVD in situ doped Si, silicon oxide, tube-type PEALD, tunnel oxide

1 | INTRODUCTION

The passivated emitter and rear cell (PERC), which was first reported in the late 1980s [1], is the current mainstream industrial crystalline silicon (*c*-Si) solar cell technology. In recent years, the PERC cells have been well developed, with a mass production average cell efficiency reaching ~23.5% in 2021 and a record efficiency of 24% achieved for commercial *p*-type Czochralski (Cz) PERC cell in 2019 [2]. However, this cell performance is approaching its practical limit [3–8] because of the recombination losses at the metal contacts and bulk [9]. In addition, as the bulk lifetime of *c*-Si wafers has been steadily improving over the years, charge carrier recombination at the cell surfaces and contacts is becoming a major bottleneck for further improving cell efficiency. Passivating contacts have been proposed for the next-generation industrial high-efficiency silicon solar cells [4, 10–12]. For example, solar cells with a tunnel oxide passivated contact (TOPCon) [10, 13–22] realized by an ultrathin tunnel oxide (silicon oxide, SiO_x, usually < 2 nm) and a heavily doped poly-crystalline silicon (poly-Si) layer have achieved a record efficiency of 25.8% [16] on *n*-type *c*-Si, 26.0% [23] on *p*-type *c*-Si, and 26.1% [24] for an interdigitated back contact solar cell. Furthermore, the TOPCon solar cell fabrication process is compatible with the well-developed PERC solar cell fabrication technology, making it ideal for upgrading existing PERC lines.

The tunnel oxide is a core element of the TOPCon solar cell. It has to reduce the minority carrier recombination, but simultaneously, it must not significantly hinder the majority carrier transport. Simulations have shown that the thickness of the tunnel oxide is rather critical [25]. A thick tunnel oxide will hamper majority carrier tunnel transport, but if the tunnel oxide is too thin, the minority carrier recombination will be too high. Therefore, achieving a uniform, ultrathin (< 2 nm) SiO_x layer with precise thickness control across the entire silicon wafer surface is crucial for the mass production of high-efficiency TOPCon solar cells. To date, researchers have explored many methods to grow SiO_x, such as thermal oxidation [26–29], wet-chemical oxidation [13, 29–31], ozone oxidation [29, 30], and plasma-assisted nitrous oxide (N_2O) oxidation [21, 32, 33]. High-quality SiO_x films have been obtained by the above methods with recombination current density (J_0) of < 10 fA/cm^2. However, most of these methods are still restricted to the lab scale, as they face challenges in mass production requirements such as uniformity, stability, and repeatability, especially for the rapid wafer size growing trends from 166 to 210 mm in recent years. Achieving a uniform thin tunnel oxide across a large wafer area is becoming increasingly challenging. Furthermore, none of these methods are able to control the tunnel oxide thickness precisely and proactively. Atomic layer deposition (ALD) is well known to allow for highly uniform deposition of thin films with accurate control of the film thickness, and its merits are already exploited in high-volume manufacturing of PERC cells for the deposition of the AlO_x layer. However, to date, ALD has not demonstrated its potential to be used as the tunnelling oxide in TOPCon solar cell applications, compared to the traditional thermal and chemical oxide. In 2020, M. Lozac'h's group fabricated the tunnel oxide using a lab-scale remote-plasma plasma-enhanced ALD (PEALD). However, their reported cell V_{oc} < 640 mV and cell efficiency < 19% were not remarkable by current standards [34, 35]. Therefore, ALD was not considered a potential method for tunnel oxide fabrication in TOPCon solar cells as, for example, evidenced by review articles by D. Yan [22] and S. W. Glunz [36] published in 2021.

Here we demonstrate a new approach with an industrial tube-based PEALD method via direct plasma technology with atomic-scale control, which can provide high-quality, dense tunnel oxide (SiO_x) films at a low cost and high throughput compared to lab-scale remote plasma technologies. In combination with an in situ doped poly-Si (n^+) layer grown using a tube-based plasma-enhanced chemical vapor deposition (PECVD) process, extremely low J_0 values of 2.8 fA/cm^2, an implied open-circuit voltage (iV_{oc}) as high as 759 mV, and resistivities (ρ_c) down to 0.6 mΩcm^2 were achieved, which are comparable to the state-of-the-art results reported by other methods as shown in Table 1. The excellent results were attributed to a uniform ultrathin SiO_x layer at the interface between *c*-Si and poly-Si (n^+) layer with a thickness of ~1.3 nm. The doping profiles measured over a large area (G12 sized wafer, 440.96 cm^2) and for different runs were almost identical, demonstrating the excellent uniformity and repeatability of the ALD technology. Moreover, when this method was applied to grow the SiO_x tunnel oxide in industrial TOPCon solar cells, a cell efficiency of 24.2% was achieved with V_{oc} as high as 710 mV. The record level passivation, excellent uniformity, repeatability, and, most importantly, precise thickness control at the atomic scale of the newly developed tube-type industrial PEALD SiO_x technology make it a potentially attractive route towards industrial mass production of high-efficiency atomic-scale controlled tunnel oxide passivated contact (ASC-TOPCon) solar cells.

The developed tube-type PEALD method for SiO_x tunnel oxide deposition can easily be integrated with tube-type PECVD systems (for n^+ doped poly-Si deposition), which are conventionally used in the manufacturing of PERC cells and are popular for its low cost of ownership (COO) because of the lower equipment cost, smaller footprint, higher uptime, and low maintenance cost. With this integrated tube-type PEALD/PECVD method, all the thin film layers in TOPCon solar cells can be deposited by one combined PEALD/PECVD system, thus enabling a completely new approach for industrial-scale high-throughput fabrication of TOPCon solar cells that replaces three separate standalone setups (for LPCVD SiO_x + LPCVD Poly + ALD Al_2O_3 + PECVD SiN_x) with just one integrated tool (tube-type PEALD SiO_x + tube-type PECVD Poly + tube-type PEALD Al_2O_3 + tube-type PECVD SiN_x), as shown in Figure 2. Like a heterojunction solar cell, one deposition tool is sufficient to complete the deposition of all

TABLE 1 Summary of the state-of-the-art J_0 and iV_{oc} results reported in the literature for different deposition methods of the interfacial SiO_x and doped poly-Si (n^+) layers on planar surfaces

Surface	Poly-Si (n^+)	Interfacial SiO_x	Post-dep. anneal	J_0 (fA/cm^2)	iV_{oc} (mV)	Ref.
Planar	LPCVD	Chemical	FGA	1.5	742	[29]
			SiN_x	0.6	747	[29]
			SiN_x	8	/	[28]
		Ozone	FGA	0.5	743	[29]
			SiN_x	0.6	748	[29]
		Thermal	SiN_x	2.2	743	[28]
			SiN_x + firing	5.2	734	[28]
			FGA	1.1	742	[29]
			SiN_x	0.8	749	[29]
	PECVD	Chemical	FGA	5	/	[27]
			SiN_x	7.1	719	[31]
			/	10.3	714	[37]
		Ozone	Hydrogen plasma	/	728	[30]
		Thermal	FGA	4.5	/	[27]
			FGA	0.9	741	[29]
			SiN_x	0.4	749	[29]
		Plasma-assisted N_2O	FGA + Al_2O_3	3	742	[21]
			AlO_x/SiN_x	2	747	[33]
	Tube-PECVD	Chemical	Hydrogen plasma	/	730	[38]
		Ozone	Hydrogen plasma	/	735	[39]
		Thermal	Hydrogen plasma	/	735	[38]
			Hydrogen plasma	1	740	[39]
		Tube-PEALD	SiN_x	2.8	759	This work
			SiN_x + firing	3.2	755	
	a-Si (n^+)	a-Si (intrinsic)	/	2	753.4	[40]

Notes: PEALD, plasma-assisted atomic layer deposition; PECVD, plasma-enhanced chemical vapor deposition; FGA, forming gas anneal.

the thin film layers, making its fabrication process more competitive than conventional methods. This integrated new approach simplifies manufacturing complexity and accelerates the mass production and commercialization of next-generation high-efficiency industrial TOPCon solar cells after PERC.

2 | EXPERIMENTAL DETAILS

To investigate the performance of the developed industrial tube-type PEALD tunnel oxide (SiO_x) at the device level, ASC-TOPCon cells were fabricated using an industrial pilot test line based on the process flow shown in Figure 1. The resulting cell structure is shown in Figure 2. G12-sized (170 μm, 440.96 cm^2) Czochralski (Cz) *n*-type silicon wafers with a resistivity of 0.3–2.1 Ω cm were used. The wafers were first saw-damage etched (SDE) in potassium hydroxide (KOH) then subjected to an alkaline texturing on both sides of the wafer, resulting in a pyramid size of ~2 μm. After cleaning, boron diffusion was performed in a tube furnace using boron trichloride (BCl_3) as a dopant source to form a p^+ layer. Subsequently, an inline single-side

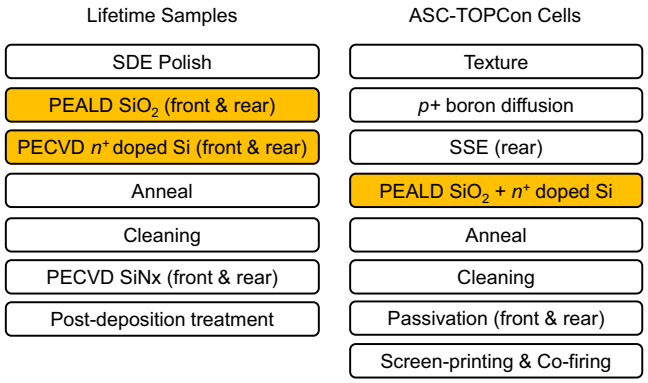

FIGURE 1 The fabrication process flows for the lifetime samples and ASC-TOPCon bifacial silicon solar cells. ASC-TOPC, atomic-scale controlled tunnel oxide passivated contact [Colour figure can be viewed at wileyonlinelibrary.com]

etch (SSE) was performed to remove the wrap-around p^+ doping at the rear surface. After cleaning, the atomic-scale controlled tunnel oxide (SiO_x) was deposited by the new industrial tube-type PEALD

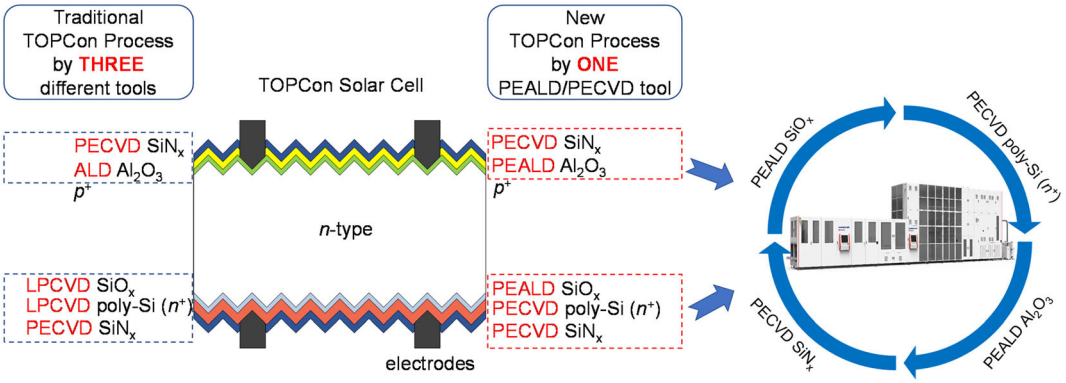

FIGURE 2 Schematic of an *n*-type ASC-TOPCon bifacial silicon solar cell with tunnel oxide enabled by newly developed tube-type PEALD SiO_x (right) versus the traditional TOPCon fabrication process (left). Furthermore, the developed tube-type PEALD process can easily be integrated with tube-type PECVD systems commonly used in the solar industry. Therefore, all thin films in TOPCon solar cells can be deposited by one combined PEALD/PECVD system, which replaces three different standalone setups in the traditional process. Photograph of the tube-type PEALD equipment courtesy of Leadmicro. ASC-TOPC, atomic-scale controlled tunnel oxide passivated contact; PEALD, plasma-assisted atomic layer deposition; PECVD, plasma-enhanced chemical vapor deposition [Colour figure can be viewed at wileyonlinelibrary.com]

system (ZR5000, LeadMicro) using 0, 1, 2, 3, 4, 5, 6, 7, and 8 ALD cycles to obtain different SiO_x thicknesses. For the PEALD SiO_x process, a proprietary silicon source was used as the metal precursor. An oxygen (O_2) plasma was used as the oxidant, generated by a direct radio frequency (RF) plasma source operating at 40 KHz at a power of 12 kW with an O_2 pressure of 120 Pa. All films were deposited at a set temperature of 200°C, and the cycle time was 25 s. The SiO_x thickness was controlled by adjusting the number of ALD cycles. The steady state ALD growth rate was ~1.2 Å/cycle, as measured by ex situ spectroscopic ellipsometry on polished samples with a 300 ALD cycle ALD SiO_x film. Subsequently, an intrinsic Si and n^+ doped Si stack layer with a thickness of around 30 and 130 nm, respectively, were deposited on PEALD SiO_x at the rear surface by a tube-type PECVD system (ZR5000, LeadMicro), using a silane and hydrogen (SiH_4 and H_2) flow mixture together with phosphine (PH_3) as the dopant source. The deposition temperature was ~ 400°C. This stack layer allows us to control the dopant concentration and distribution after the high-temperature annealing. All samples were then annealed in a tube furnace at 920°C for 45 min to facilitate crystallization and dopant activation, forming a n^+ doped polysilicon (poly-Si) layer. Subsequently, an inline SSE was performed to remove the wrap-around n^+ layer at the front surface. After cleaning, the front p^+ surface was passivated by a thin-film stack consisting of a ~ 3 nm PEALD Al_2O_3 film and a ~ 70 nm PECVD SiN_x film, whereas the rear surface was coated with a ~ 70 nm SiN_x film. An industrial tube-type PEALD/PECVD system (ZR5000, LeadMicro) deposited all the thin films. Lastly, the samples were screen-printed on both sides with an Al-Ag alloy paste for the front electrodes and Ag paste for the rear electrodes. The cells were then fired at a peak temperature of around 800°C using an industrial fast-firing furnace (set temperature, unless stated otherwise). No blistering effect was observed in this work.

To evaluate the level of surface passivation of the tunnel oxide (by tube-type PEALD SiO_x) and n^+ doped poly-Si (by tube-type PECVD) stacks, symmetrical lifetime samples were prepared based on the process flow shown in Figure 1. The same G12-sized Cz *n*-type silicon wafers were used. After SDE and cleaning, a polished surface was formed on both sides. Subsequently, 5 cycles of PEALD SiO_x were deposited on both sides of the samples. An intrinsic Si/n^+ doped Si stack layer was then deposited on both sides of the samples by PECVD, followed by an anneal process as described earlier. In this way, a symmetrical structure of poly-Si (n^+)/SiO_x/Si (*n*)/SiO_x/poly-Si (n^+) was formed. After cleaning, a ~ 70 nm SiN_x film was deposited on both sides of the samples by PECVD. Finally, the symmetrical samples underwent a rapid thermal anneal in an industrial fast firing furnace with a set peak temperature of 800°C.

The passivation quality was quantified by measuring the effective minority carrier lifetime of the symmetrical samples using a contactless photoconductance decay tester (WCT-120, Sinton Instruments). The iV_{oc} of the samples was extracted accordingly using the method proposed by Sinton and Cuevas [41]. The single-side J_0 was determined according to the high-injection method proposed by Kane and Swanson [42]:

$$\frac{1}{\tau_{eff}} - \frac{1}{\tau_{Auger}} = \frac{1}{\tau_{SRH}} + \frac{2J_o(N_d + \Delta n)}{qn_i^2 W} \quad (1)$$

where τ_{eff} is the measured effective carrier lifetime of the sample, τ_{Auger} is the intrinsic Auger lifetime [43], τ_{SRH} is the defect-related Shockley–Read–Hall bulk lifetime, N_d is the bulk doping concentration, Δn is the excess carrier density, q is the elementary charge, n_i is the intrinsic carrier concentration, and W is the sample thickness. The active dopant depth profile was measured by electrochemical capacitance-voltage profiling (ECV, WEP, CVP21). The contact resistivity was measured by the transmission line method (TLM, Ai-shine). The structural and chemical composition of the *c*-Si/SiO_x/poly-Si(n^+) interface was investigated by transmission electron microscopy (TEM, FEI Talos and Titan) energy-dispersive X-ray spectroscopy (EDS) in combination with scanning TEM electron energy loss spectroscopy (STEM EELS). The EELS spectra were processed by background

subtraction followed by a Fourier-log deconvolution to remove plural scattering contributions. Full-area current–voltage (*I*–*V*) measurements were conducted using a *Halm* inline measurement system with a calibrated reference cell from Fujian Metrology Institute, National PV Industry Measurement and Testing Center.

3 | RESULTS AND DISCUSSION

3.1 | Passivation properties of the SiO_x/poly-Si(n^+) films enabled by tube-type PEALD/PECVD techniques

The phosphorus doping profile of the n^+ layer depends on many factors, such as the tunnel oxide stoichiometry and thickness, poly-Si thickness, deposition recipes, in situ doping recipes, annealing recipes, etc. [28, 30, 44]. The active phosphorus doping profile of the n^+ layer by the tube-type PECVD process on PEALD SiO_x (5 ALD cycles) used in this work is shown in Figure 3. For comparison, the phosphorus doping profile by the traditional LPCVD method (thermal SiO_x + intrinsic polysilicon + phosphorus diffusion) is also shown in Figure 3 as a reference. As can be seen from Figure 3, the doping profile was almost identical over a large area between the center and the edge of a G12-sized wafer (440.96 cm^2, one of the largest commercial wafers in the market), as well as for repeated runs (Run 1 versus Run 2). This clearly demonstrates the key advantages of tube-type PEALD SiO_x technology (shares all the intrinsic advantages of ALD technology) in achieving precise thickness control, excellent thickness uniformity, and consistent oxide quality over large areas and different runs, making it an ideal deposition method for atomic-scale control of the tunnel oxide in favor of manufacturing requirements [45, 46], compared to other tunnel oxide formation methods. A peak doping concentration of $\sim 5 \times 10^{20}$ cm^{-3} and a junction depth of ~120 nm was achieved. Compared to the doping level of the LPCVD reference ($\sim 2 \times 10^{20}$ cm^{-3}), the doping level afforded by the in situ doped PECVD method is significantly higher. Firstly, higher dopant concentration generally results in better J_0 and better contact resistivity (ρ_c) [28, 47, 48]. Contact resistivity values of ~ 1 mΩcm^2 could be obtained for doping levels ($N_{poly\text{-}Si}$) > 1×10^{20} cm^{-3} [48]. It should be noted that such a high doping level does not interfere with the surface passivation of SiO_x/poly-Si (n^+) structure as the tunnel oxide is an effective diffusion barrier [48]. However, the high dopant concentration could also adversely affect the infrared response of silicon solar cells via free-carrier absorption [39, 49]. Secondly, J_0 could significantly increase, leading to an increased Auger recombination if there is excessive diffusion of dopants from the poly-Si layer through the oxide into the *c*-Si, which may occur at high annealing temperatures if the oxide is too thin, or for other process reasons [28, 47]. This work shows that tube-type PEALD SiO_x can serve as an effective diffusion barrier, as can be seen from the tail of the doping profile.

Apart from the doping profiles, hydrogenation is another key process for enabling record-high surface passivation quality. The tunnel oxide is very thin in TOPCon applications; the interface defect density could be higher than thicker SiO_x layers. A hydrogenation step could effectively reduce the defects at the SiO_x/*c*-Si interface [48, 50] and also possibly the defects within the poly-Si layer [51]. In this work, hydrogenation by a tube-type PECVD SiN_x capping layer [28, 52] was found to be very effective. The measured effective lifetime, together with the corresponding iV_{oc} and single-side J_0, results for the symmetrically passivated samples before and after firing is shown in Figure 4. An average effective lifetime value of 5.3 and 5 ms were obtained before and after firing, respectively, and a champion lifetime of 7.2 ms was obtained. It can be seen that good passivation had been achieved before firing, although the firing process slightly deteriorated the passivation quality. A similar finding was reported by Feldmann et al., whereby the high-temperature firing process deteriorated the surface passivation of a TOPCon cell compared to a low temperature (425°C) forming gas anneal process [30, 48]. It was also reported that poly-Si junctions grown on thicker and denser interfacial oxides with optimum annealing temperatures above 900°C exhibit excellent passivation quality directly after junction formation [4, 53]. In our ASC-TOPCon cells, it was observed that the distribution of the passivation results became narrower after firing and reached a stable condition (higher lifetime samples had reduced surface passivation, and lower lifetime samples had improved surface passivation after firing). J_0 values as low as 2.8 fA/cm^2 and iV_{oc} values as high as 759 mV were achieved. The results are comparable to the state-of-the-art J_0 results < 10 fA/cm^2 reported by other growth methods such as interfacial SiO_x layer grown by thermal oxidation [26–29], wet-chemical oxidation [13, 29–31], ozone oxidation [29, 30], or plasma-assisted nitrous oxide (N_2O) oxidation [21, 32, 33] capped with poly-Si (n^+) by LPCVD [26, 28, 29, 54] or PECVD [13, 27, 29, 31, 37, 55], as shown in Table 1. The results are also comparable to a-Si (intrinsic)/a-Si (n^+) stacks with J_0 values as low as 2 fA/cm^2 [4, 40]. The results, therefore, are evidence of an excellent passivation capability attained by the industrial tube-type PEALD SiO_x tunnel oxide and PECVD in situ doped poly-Si (n^+) structure developed in this work.

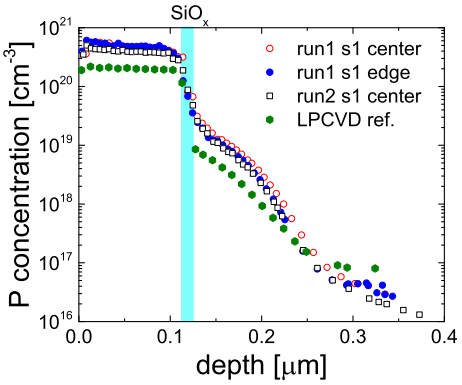

FIGURE 3 Active phosphorus doping profile of the n^+ layer by the tube-type PECVD process on PEALD SiO_x (5 ALD cycles) in an ASC-TOPCon cell. The phosphorus doping profile by the traditional LPCVD method (thermal SiO_x + intrinsic polysilicon + phosphorus diffusion) is shown as a reference. ASC-TOPC, atomic-scale controlled tunnel oxide passivated contact; PEALD, plasma-assisted atomic layer deposition; PECVD, plasma-enhanced chemical vapor deposition [Colour figure can be viewed at wileyonlinelibrary.com]

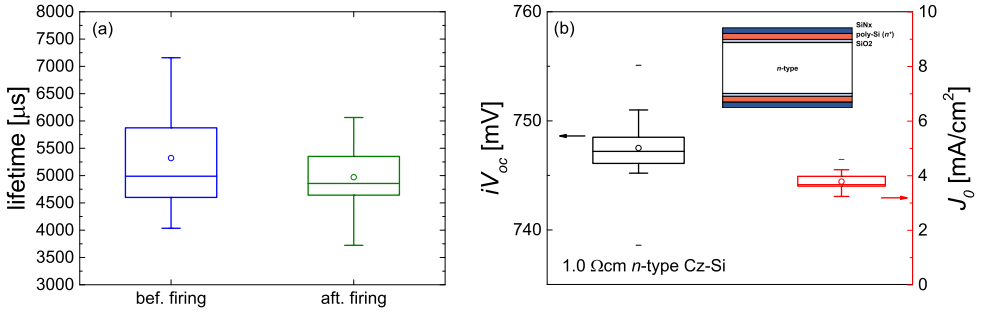

FIGURE 4 (a) Measured effective lifetime of symmetrical passivated samples before and after firing, (b) measured iV_{oc} values (left axis) and single-side J_0 values (right axis) of symmetrical passivated samples after firing. A schematic of the symmetrical passivated sample is shown in the inset of (b), where both front and back sides are coated with PEALD SiO_x (5 cycles)/PECVD n^+ doped poly-Si (130 nm)/SiN_x (70 nm). Four wafers were measured with five points measured on each wafer (center and four corners). Boxes, 25–75% range; vertical lines, maximum and minimum; horizontal lines within boxes, median; circle shape within boxes, mean. PEALD, plasma-assisted atomic layer deposition; PECVD, plasma-enhanced chemical vapor deposition [Colour figure can be viewed at wileyonlinelibrary.com]

3.2 | Structural and chemical characterization of the c-Si/SiO_x/poly-Si (n^+) interface

To visualize the *c*-Si/SiO_x/poly-Si(n^+) interface, we performed cross-section TEM imaging, as shown in Figure 5a. The results show evidence for the existence of a uniform amorphous SiO_x layer of ~1.3 nm at the interface between the crystalline Si substrate and the poly-crystalline Si (n^+) layer [34, 56]. It includes the native oxide prior to ALD oxide growth. The degree of crystallinity of the poly-Si layer after annealing in this work was about 92% as determined by Raman measurements (results not shown here). To further analyze the chemical composition of the ultrathin interface layer, TEM EDS mapping and line scans were carried out across the interface as shown in Figure 5b and c, respectively. The EDS results show that the ultrathin interface layer mainly consists of SiO_x. However, the actual thickness from the line scan appears thicker than ~1.3 nm measured in the cross-section image. This could be because of beam broadening effects that occur because of electron scattering within the sample volume or possible sample drift while the line scan was being measured. STEM EELS line scan was also carried out to corroborate the chemical characterization results from EDS. A 3D plot of the EELS low loss spectra taken at 100 points along a 10 nm line scan (Figure 5d) shows the variation of the intensity of the Si plasmon loss peak (at ~17 eV) as the scan is performed from the *c*-Si to SiO_x to poly-Si regions (position 1 to position 100). A secondary peak at ~23.5 eV can also be observed throughout the line scan. This peak can be attributed to either the SiO_x plasmonic peak [57] or the phosphorus plasmonic peak [58], which have similar energy loss values. We attribute the secondary peak in the *c*-Si and poly-Si (n^+) regions to phosphorus and the secondary peak in the SiO_x region to SiO_x. The SiO_x region is therefore revealed by the decrease in intensity of the Si plasmon peak. The individual EELS spectra at points 1, 58, and 100 are presented in Figure 5e, representing the spectra taken in the *c*-Si, SiO_x, and poly-Si regions, respectively. Like the EDS line scan results in Figure 5c, a larger apparent SiO_x thickness (region with low Si plasmon peak intensity) in the EELS line scan could be because of possible sample drift while the line scan was being measured.

3.3 | Solar cell performance

To verify the performance of the developed atomic-scale controlled tunnel oxide by industrial tube-type PEALD SiO_x at the device level, ASC-TOPCon cells were fabricated based on the process flow shown in Figure 1. PEALD SiO_x grown using 5 ALD cycles was used as baseline. To investigate the influence of the tunnel oxide at atomic level, PEALD SiO_x with 0 to 8 ALD cycles were used for comparison. Please note that this work optimized the PECVD in situ doped Si (n^+) and the annealing processes for the SiO_x thickness obtained with 5 ALD cycles. By tuning these two processes, good results can also be achieved for thicker SiO_x with more ALD cycles (results not shown here). The solar cell performance was evaluated using relevant metrics, and the data are shown in Figure 6. The best result with average cell efficiency of 24% was obtained for the baseline group with 5 ALD cycles. Similar results with average cell efficiency of 24% were obtained for 6 ALD cycles without tuning the process parameters for doped-Si (n^+) growth and the annealing step. The average cell efficiency dropped significantly for lower tunnel oxide thickness (< 5 ALD cycles). The main contributors to this decreased cell efficiency are a significant drop in V_{oc} and a lower fill factor (FF). This could be because for the thinner tunnel oxide, more phosphorus dopants diffuse from the poly-Si (n^+) layer into the *c*-Si layer, which might lead to increased Auger recombination and increased minority carrier recombination. For thicker tunnel oxide thickness (> 6 ALD cycles), the average cell efficiency also declined significantly, with the main contributors to the reduced cell efficiency being FF (dropped from the baseline of 83.8% to 82.7% for 8 ALD cycles), followed by a smaller V_{oc}. This could be because of a reduced tunnelling effect with a thicker tunnel oxide. Nevertheless, at 5 ALD cycles of SiO_x growth, a cell efficiency of 24.2% was achieved for the ASC-TOPCon solar cell with a V_{oc} as high as 710 mV, and an average ρ_c of the rear side of

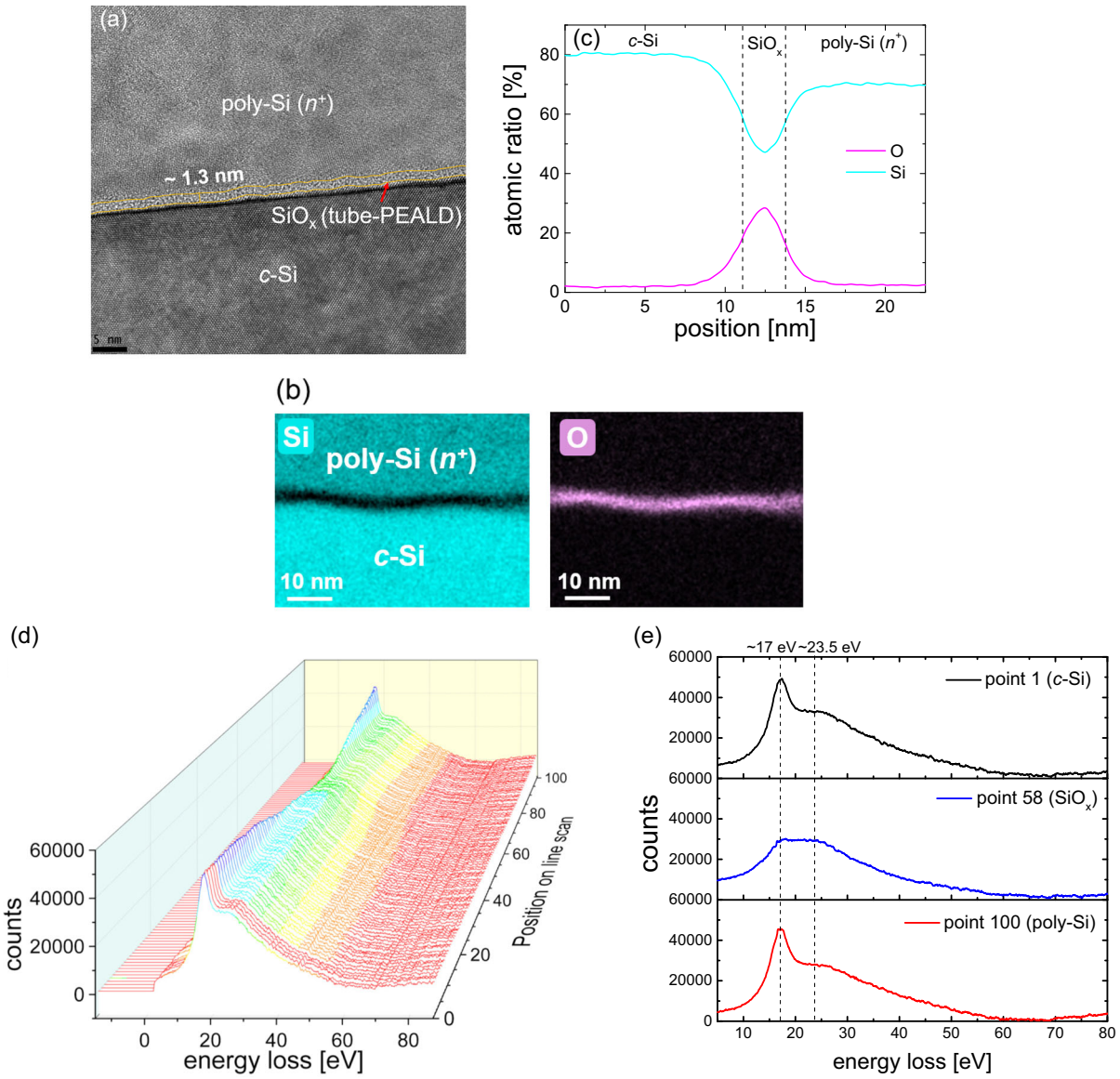

FIGURE 5 (a) Cross-sectional TEM image of the rear interface (cell precursor before metallization) with tube-type PEALD tunnel SiO_x (5 ALD cycles) and PECVD in situ doped poly-Si (n^+) stack. (b) TEM-EDS mapping across the rear interface shows Si and O detected in the region. A strong O signal was detected in the SiO_x region. (c) The EDS line scan across the rear interface shows the Si and O atomic ratio variation at the different regions. (d) The 3D plot of 100 STEM EELS low loss spectra captured during the line scan across the c-Si/SiO_x/poly-Si (n^+) interface (point 1 in c-Si and point 100 in poly-Si), showing the variation of the Si plasmon peak intensity. (e) Individual EELS low loss spectra of the Si plasmon peak region at points 0 (c-Si), 58 (SiO_x), and 100 (poly-Si). PEALD, plasma-assisted atomic layer deposition; PECVD, plasma-enhanced chemical vapor deposition; FGA, forming gas anneal, TEM, transmission electron microscopy; EDS, energy-dispersive X-ray spectroscopy; STEM EELS, scanning TEM electron energy loss spectroscopy [Colour figure can be viewed at wileyonlinelibrary.com]

about 0.94 mΩcm^2 measured by the TLM method. It demonstrates that such an excellent cell performance can be obtained with the newly developed PEALD SiO_x technology and thus opens a new route for mass production of high-efficiency industrial TOPCon solar cells.

Moreover, this work shows that the process window for the tunnel oxide is about 2 ALD cycles within 2.4 Å. With this narrow process window, it goes to show that it is essential to control the tunnel oxide thickness precisely to meet the stringent requirements for high-efficiency TOPCon solar cell mass production.

3.4 | ASC-TOPCon module performance

To further evaluate the performance of the developed ASC-TOPCon solar cells at the module level, ASC-TOPCon modules consisting of 60 pieces of ASC-TOPCon cells (G12-sized wafer, 440.96 cm^2) were fabricated. ASC-TOPCon cells with cell efficiencies between 24% to 24.2% were used. A PERC module (G12-sized wafer, 440.96 cm^2 with cell efficiency of 22.8% from the production line, 60 cells) was fabricated as a reference. The cells were half-cut by laser and double-side

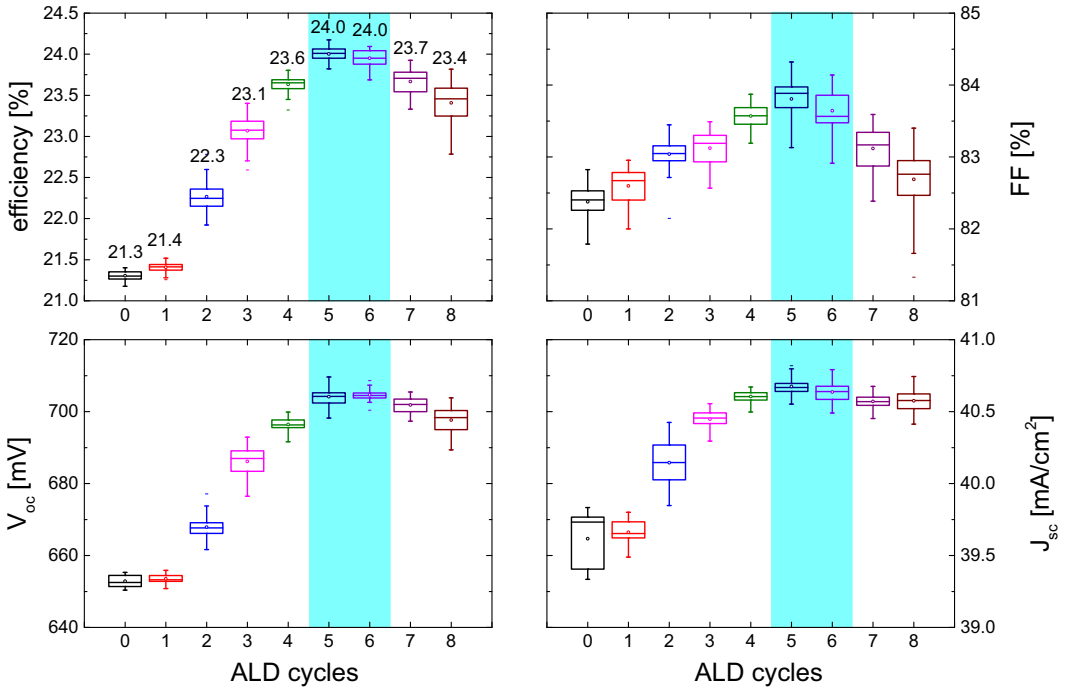

FIGURE 6 Cell performance metrics of ASC-TOPCon samples with 0 to 8 cycles of PEALD SiO_x tunnel oxide. Boxes, 25–75% range; vertical lines, maximum and minimum; horizontal lines within boxes, median; circle shape within boxes, mean. ASC-TOPC, atomic-scale controlled tunnel oxide passivated contact; PEALD, plasma-assisted atomic layer deposition [Colour figure can be viewed at wileyonlinelibrary.com]

Module with 60 cells	Cell efficiency (%)	P_{max} (W)	V_{oc} (V)	I_{sc} (A)	FF (%)
ASC-TOPCon 1	24.0%	609.7	42.52	17.68	81.1
ASC-TOPCon 2	24.1%	611.7	42.53	17.76	81.0
ASC-TOPCon 3	24.1%	611.6	42.55	17.76	81.0
ASC-TOPCon 4	24.2%	612.9	42.65	17.74	81.0
PERC Reference	22.8%	595.6	41.21	18.17	79.5
Max (TOPCon-PERC)		17.3			

TABLE 2 I–V results for the ASC-TOPCon modules with illumination from the front side

laminated with two tempered glass panels to form bifacial modules. The modules were measured by an in-line module tester, using a reference module of the same cell technology calibrated in TÜV Rheinland and the rear side of the module is covered with a black sheet. The results are shown in Table 2. Over 600 W power was achieved with a champion module power of 613 W. About 17 W higher compared to the PERC baseline reference. This demonstrated the potential of ASC-TOPCon modules.

4 | CONCLUSION

In conclusion, we have shown that a new tube-type industrial PEALD technique can achieve precise control of a SiO_x tunnel oxide at the atomic scale. In combination with a PECVD in situ doped poly-Si (n^+) layer, excellent passivation was achieved with an effective lifetime above 7 ms. Moreover, extremely low recombination current densities down to 2.8 fA/cm^2 and implied open-circuit voltage as high as 759 mV were obtained, which are comparable to the state-of-the-art results reported by other interfacial SiO_x growth methods, as well as for a-Si (intrinsic)/a-Si (n^+) stacks. TEM EDS and STEM EELS measurements proved the existence of a uniform $\sim$ 1.3 nm SiO_x layer at the interface between the *c*-Si and poly-Si (n^+) layer. The almost identical doping profiles over a large size wafer (G12-sized wafer, 440.96 cm^2) and for repeated runs demonstrated the excellent uniformity and repeatability of the PEALD technology. The developed tube-type PEALD SiO_x with 0 to 8 ALD cycles was applied to industrial ASC-TOPCon solar cells, yielding a cell efficiency of 24.2% with an open-circuit voltage as high as 710 mV and an average rear side contact resistivity of about 0.94 mΩcm^2. The cell results were strongly dependent on the number of ALD cycles. The process window for the tunnel oxide was about 2 ALD cycles within 2.4 Å, highlighting the importance of precise thickness control of the tunnel oxide at the atomic scale to meet the stringent requirements for high-efficiency TOPCon solar cell mass production. The record level passivation, excellent uniformity, repeatability, and precise thickness control at the

atomic scale of the developed tube-type industrial PEALD SiO_x technology thus open a new route for the mass production of high-efficiency industrial ASC-TOPCon solar cells. ASC-TOPCon modules were fabricated and gave a maximum power of more than 17 W higher than the PERC reference module with PERC cells from the production line, which demonstrated the potential of the ASC-TOPCon enabled by the novel tube-type PEALD technologies. Furthermore, the developed tube-type PEALD method can easily be integrated with tube-type PECVD systems commonly used in the solar industry. Therefore, all thin films in TOPCon solar cells can be deposited by one integrated PEALD/PECVD system. This completely new approach could thus significantly simplify the manufacturing complexity and foster the commercialization of next-generation high-efficiency industrial TOPCon solar cells.

ACKNOWLEDGEMENTS

The authors acknowledge the support from the industrial partners. This research is supported by the Research Funding for High-level Talents of Nantong University (No. 03083035), the Major Program for the Natural Science Research of the Higher Education Institutions of Jiangsu Province, China (No. 19KJ320004), and the Construction Fund for School of Tongke Microelectronics, Nantong University (No. 0702610104). B. L. acknowledges the support of the "Distinguished Professor of Jiangsu Province" award.

DATA AVAILABILITY STATEMENT

The data that support the findings of this study are available from the corresponding author upon reasonable request.

ORCID

Baochen Liao https://orcid.org/0000-0003-2860-8942
Xinyuan Wu https://orcid.org/0000-0002-7908-3296

REFERENCES

1. Blakers AW, Wang A, Milne AM, Zhao J, Green MA. 22.8% efficient silicon solar cell. *Appl Phys Lett*. 1989;55:1363-1365.
2. Green MA, Dunlop ED, Hohl-Ebinger J, Yoshita M, Kopidakis N, Hao X. Solar cell efficiency tables (version 58). *Progr Photovolt: Res Appl*. 2021;29:657-667.
3. Min B, Müller M, Wagner H, et al. A roadmap toward 24% efficient PERC solar cells in industrial mass production. *IEEE J Photovolt*. 2017;7:1541-1550.
4. Schmidt J, Peibst R, Brendel R. Surface passivation of crystalline silicon solar cells: present and future. *Solar Energy Mater Solar Cells*. 2018;187:39-54.
5. Saint-Cast P, Werner S, Greulich J, et al. Analysis of the losses of industrial-type PERC solar cells. *Phys Stat Solidi A*. 2017;214:1600708.
6. Huang H, Lv J, Bao Y, et al. 20.8% industrial PERC solar cell: ALD Al2O3 rear surface passivation, efficiency loss mechanisms analysis and roadmap to 24%. *Solar Energy Mater Solar Cells*. 2017;161:14-30.
7. Müller M, Fischer G, Bitnar B, et al. Loss analysis of 22% efficient industrial PERC solar cells. *Energy Procedia*. 2017;124:131-137.
8. Zhao J, Wang A, Green MA. 24 5% efficiency silicon PERT cells on MCZ substrates and 24·7% efficiency PERL cells on FZ substrates. *Progr Photovolt: Res Appl*. 1999;7:471-474.
9. Altermatt PP, Yang Y, Chen Y, et al. Learning from the past to look beyond the roadmap of PERC Si solar cell mass production. In: *35th European Photovoltaic Solar Energy Conference and Exhibition*, Brussels, Belgium; 2018:215-221.
10. Feldmann F, Simon M, Bivour M, Reichel C, Hermle M, Glunz SW. Carrier-selective contacts for Si solar cells. *Appl Phys Lett*. 2014;104:181105.
11. Melskens J, van de Loo BWH, Macco B, Black LE, Smit S, Kessels WMM. Passivating contacts for crystalline silicon solar cells: from concepts and materials to prospects. *IEEE J Photovolt*. 2018;8:373-388.
12. Allen TG, Bullock J, Yang X, Javey A, De Wolf S. Passivating contacts for crystalline silicon solar cells. *Nat Energy*. 2019;4:914-928.
13. Feldmann F, Bivour M, Reichel C, Hermle M, Glunz SW. Passivated rear contacts for high-efficiency n-type Si solar cells providing high interface passivation quality and excellent transport characteristics. *Solar Energy Mater Solar Cells*. 2014;120:270-274.
14. Feldmann F, Bivour M, Reichel C, Steinkemper H, Hermle M, Glunz SW. Tunnel oxide passivated contacts as an alternative to partial rear contacts. *Solar Energy Mater Solar Cells*. 2014;131:46-50.
15. Römer U, Peibst R, Ohrdes T, et al. Recombination behavior and contact resistance of n+ and p+ poly-crystalline Si/mono-crystalline Si junctions. *Solar Energy Mater Solar Cells*. 2014;131:85-91.
16. Richter A, Benick J, Feldmann F, Fell A, Hermle M, Glunz SW. N-type Si solar cells with passivating electron contact: identifying sources for efficiency limitations by wafer thickness and resistivity variation. *Solar Energy Mater Solar Cells*. 2017;173:96-105.
17. Yan D, Phang SP, Wan Y, Samundsett C, Macdonald D, Cuevas A. High efficiency n-type silicon solar cells with passivating contacts based on PECVD silicon films doped by phosphorus diffusion. *Solar Energy Mater Solar Cells*. 2019;193:80-84.
18. Chen D, Chen Y, Wang Z, et al. 24.58% total area efficiency of screen-printed, large area industrial silicon solar cells with the tunnel oxide passivated contacts (i-TOPCon) design. *Solar Energy Mater Solar Cells*. 2020;206:110258.
19. Chen W, Truong TN, Nguyen HT, et al. Influence of PECVD deposition temperature on phosphorus doped poly-silicon passivating contacts. *Solar Energy Mater Solar Cells*. 2020;206:110348.
20. Nandakumar N, Rodriguez J, Kluge T, et al. Approaching 23% with large-area monopoly cells using screen-printed and fired rear passivating contacts fabricated by inline PECVD. *Progr Photovolt: Res Appl*. 2018;27:107-112.
21. Gao T, Gao T, Yang Q, et al. An industrially viable TOPCon structure with both ultra-thin SiOx and n+−poly-Si processed by PECVD for p-type c-Si solar cells. *Solar Energy Mater Solar Cells*. 2019;200:109926.
22. Yan D, Cuevas A, Michel JI, et al. Polysilicon passivated junctions: the next technology for silicon solar cells? *Joule*. 2021;5:811-828.
23. Richter A, Müller R, Benick J, et al. Design rules for high-efficiency both-sides-contacted silicon solar cells with balanced charge carrier transport and recombination losses. *Nat Energy*. 2021;6:429-438.
24. Haase F, Hollemann C, Schäfer S, et al. Laser contact openings for local poly-Si-metal contacts enabling 26.1%-efficient POLO-IBC solar cells. *Solar Energy Mater Solar Cells*. 2018;186:184-193.
25. Steinkemper H, Feldmann F, Bivour M, Hermle M. Numerical simulation of carrier-selective electron contacts featuring tunnel oxides. *IEEE J Photovolt*. 2015;5:1348-1356.
26. Romer U, Peibst R, Ohrdes T, et al. Ion implantation for poly-Si passivated Back-junction back-contacted solar cells. *IEEE J Photovolt*. 2015;5:507-514.
27. Yan D, Cuevas A, Bullock J, Wan Y, Samundsett C. Phosphorus-diffused polysilicon contacts for solar cells. *Solar Energy Mater Solar Cells*. 2015;142:75-82.
28. Stodolny MK, Lenes M, Wu Y, et al. N-type polysilicon passivating contact for industrial bifacial n-type solar cells. *Solar Energy Mater Solar Cells*. 2016;158:24-28.

29. Peibst R, Larionova Y, Reiter S, et al. Implementation of n+ and p+ POLO junctions on front and rear side of double-side contacted industrial silicon solar cells. In: *presented at the 32nd Europ. Photovolt. Sol. Energy Conference*, Munich, Germany; 2016.
30. Moldovan A, Feldmann F, Zimmer M, Rentsch J, Benick J, Hermle M. Tunnel oxide passivated carrier-selective contacts based on ultra-thin SiO_2 layers. *Solar Energy Mater Solar Cells*. 2015;142:123-127.
31. Richter A, Benick J, Müller R, et al. Tunnel oxide passivating electron contacts as full-area rear emitter of high-efficiency p-type silicon solar cells. *Progr Photovolt: Res Appl*. 2018;26:579-586.
32. Jeon M, Kang J, Shim G, et al. Passivation effect of tunnel oxide grown by N_2O plasma for c-Si solar cell applications. *Vacuum*. 2017; 141:152-156.
33. Huang Y, Liao M, Wang Z, et al. Ultrathin silicon oxide prepared by in-line plasma-assisted N_2O oxidation (PANO) and the application for n-type polysilicon passivated contact. *Solar Energy Mater Solar Cells*. 2020;208:110389.
34. Lozac'h M, Nunomura S, Matsubara K. Double-sided TOPCon solar cells on textured wafer with ALD SiOx layer. *Solar Energy Mater Solar Cells*. 2020;207:110357.
35. Lozac'h M, Nunomura S. Role of silicon surface, polished ⟨100⟩ and ⟨111⟩ or textured, on the efficiency of double-sided TOPCon solar cells. *Progr Photovolt: Res Appl*. 2020;28:1001-1011.
36. Glunz SW, Steinhauser B, Polzin J-I, et al. Silicon-based passivating contacts: The TOPCon route. *Progr Photovolt: Res Appl*. 2021;1-19.
37. Tao Y, Upadhyaya V, Chen C-W, et al. Large area tunnel oxide passivated rear contact n-type Si solar cells with 21.2% efficiency. *Progr Photovolt: Res Appl*. 2016;24:830-835.
38. Steinhauser B, Polzin J-I, Feldmann F, Hermle M, Glunz SW. Excellent surface passivation quality on crystalline silicon using industrial-scale direct-plasma TOPCon deposition technology. *Solar RRL*. 2018;2: 1800068.
39. Feldmann F, Steinhauser B, Pernau T, et al. Industrial TOPCon solar cells realized by a PECVD tube process. In: *37th European PV Solar Energy Conference and Exhibition*; 2020.
40. Herasimenka SY, Dauksher WJ, Bowden SG. >750 mV open circuit voltage measured on 50 μm thick silicon heterojunction solar cell. *Appl Phys Lett*. 2013;103:053511.
41. Sinton RA, Cuevas A. Contactless determination of current–voltage characteristics and minority-carrier lifetimes in semiconductors from quasi-steady-state photoconductance data. *Appl Phys Lett*. 1996;69: 2510.
42. Kane DE, Swanson RM. Measurement of the emitter saturation current by a contactless photoconductivity decay method. In: *18th IEEE PVSC*, Las Vegas, USA; 1985:578-583.
43. Sinton RA, Swanson RM. Recombination in highly injected silicon. *IEEE Trans Electron Devices*. 1987;ED-34:1380-1389.
44. Polzin J-I, Lange S, Richter S, et al. Temperature-induced stoichiometric changes in thermally grown interfacial oxide in tunnel-oxide passivating contacts. *Solar Energy Mater Solar Cells*. 2020;218:110713.
45. Johnson RW, Hultqvist A, Bent SF. A brief review of atomic layer deposition: from fundamentals to applications. *Mater Today*. 2014;17: 236-246.
46. George SM. Atomic layer deposition: an overview. *Chem Rev*. 2010; 110:111-131.
47. Geerligs LJ, Stodolny M, Wu Y, et al. LPCVD polysilicon passivating contacts. In: *Workshop on Crystalline Silicon Solar Cells and Modules: Materials and processes*. Colorado, USA: Vail; 2016.
48. Feldmann F, Fellmeth T, Steinhauser B, et al. Large area TOPCon cells realized by a PECVD tube process. In: *presented at the 36th European PV solar energy conference and exhibition*, Marseille, France, 9–13 September, 2019.
49. Feldmann F, Nicolai M, Muller R, Reichel C, Hermle M. Optical and electrical characterization of poly-Si/SiOx contacts and their implications on solar cell design. *Energy Procedia*. 2017;124:31-37.
50. Schnabel M, van de Loo BWH, Nemeth W, et al. Hydrogen passivation of poly-Si/SiOx contacts for Si solar cells using Al2O3 studied with deuterium. *Appl Phys Lett*. 2018;112:203901.
51. Truong TN, Yan D, Samundsett C, et al. Hydrogenation of phosphorus-doped polycrystalline silicon films for passivating contact solar cells. *ACS Appl Mater Interfaces*. 2019;11:5554-5560.
52. Steinhauser B, Feldmann F, Ourinson D, Nagel H, Fellmeth T, Hermle M. On the influence of the SiNx composition on the firing stability of Poly-Si/SiNx stacks. *Phys Stat Solidi A*. 2020;217:2000333.
53. Haase F, Kiefer F, Schäfer S, et al. Interdigitated back contact solar cells with polycrystalline silicon on oxide passivating contacts for both polarities. *Jpn J Appl Phys*. 2017;56:08MB15.
54. Mack S, Schube J, Fellmeth T, Feldmann F, Lenes M, Luchies J-M. Metallisation of boron-doped polysilicon layers by screen printed silver pastes. *Phys Stat Solidi (RRL) - Rapid Res Lett*. 2017;11:1700334.
55. Young DL, Nemeth W, LaSalvia V, et al. Low-cost plasma immersion ion implantation doping for interdigitated back passivated contact (IBPC) solar cells. *Solar Energy Mater Solar Cells*. 2016;158:68-76.
56. Stuckelberger J, Nogay G, Wyss P, et al. Passivating electron contact based on highly crystalline nanostructured silicon oxide layers for silicon solar cells. *Solar Energy Mater Solar Cells*. 2016;158:2-10.
57. Cuony P, Alexander DTL, Perez-Wurf I, et al. Silicon filaments in silicon oxide for next-generation photovoltaics. *Adv Mater*. 2012;24: 1182-1186.
58. Nicotra G, van Veen E, Deretzis I, et al. Anisotropic ultraviolet-plasmon dispersion in black phosphorus. *Nanoscale*. 2018;10:21918-21927.

How to cite this article: Liao B, Wu W, Yeo RJ, et al. Atomic scale controlled tunnel oxide enabled by a novel industrial tube-based PEALD technology with demonstrated commercial TOPCon cell efficiencies > 24%. *Prog Photovolt Res Appl*. 2022; 1-10. doi:10.1002/pip.3627